Infrared Physics & Technology 67 (2014) 315–317

Contents lists available at ScienceDirect

Infrared Physics & Technology

journal homepage: www.elsevier.com/locate/infrared

MWIR imaging experiments with large *F*-number optics on LEO spacecraft

Yingqi Liu [a,*], Qingyun Yang [a], Junchi Liu [a,b], Bin Wang [a], Zhenduo Zhang [a], Haojing Wang [a]

[a] Changchun Institute of Optics, Fine Mechanics and Physics, Chinese Academy of Sciences, Changchun 130033, China
[b] Graduate School of Chinese Academy of Sciences, Beijing 100039, China

HIGHLIGHTS

- Superresolution imaging used to enhance the blurred images induced by undersampling has limited capacity.
- The SNR of large *F*-number MWIR imaging for LEO extended spacecraft is sufficient under right conditions.
- We have successfully developed a large *F*-number infrared camera with cold stop matched applied on a 1.23 m telescope.
- We report some MWIR imaging experiment results about typical LEO spacecraft.

ARTICLE INFO

Article history:
Received 25 July 2014
Available online 12 August 2014

Keywords:
Infrared imaging
Telescopes
Detection
Astronomical optics

ABSTRACT

To determine the feasibility of spacecraft imaging in the mid-infrared region (3.0–5.0 μm) utilizing large *F*-number optics, we create a radiometric simulation of a low-Earth orbit (LEO) extended object, imaging background and noise, in order to predict the signal-to-noise ratio of such objects as viewed from a telescope during the daytime and terminator, etc. We find that the observation of Space Station and other extended targets utilizing large *F*-number optics for MWIR imaging is possible, given the right conditions. We have developed a large *F*-number infrared camera with cold stop matched, which is successfully applied to acquire LEO extended object images taken by a 1.23 m telescope. We get clear images of International Space Station, Tian-gong, etc. and our proposed the infrared imaging technology can be demonstrated to greatly improve the imaging ability of current ground-based Optoelectric (OE) telescope for the detection of space activities.

Ground-based OE sites routinely acquire resolved images of spacecraft, yielding a great deal of information about orbiting spacecraft. In particular, the Air Force Maui Optical and Supercomputing (AMOS) Detachment on Maui has been acquiring optical imagery using two work-horse imagery systems [1]. The AMOS Advanced Electro-optical System (AEOS) 3.6 m telescope provides visible-band with adaptive optics compensation to remove atmospheric blurring and long-wavelength thermal infrared images (Fig. 1(a) and (b)) [2]. In addition, the AMOS Gemini 1.6 m telescope system provides daytime near-infrared speckle images (Fig. 1(c)) [3]. These systems reveal a great deal of resolvable detail for spacecraft in low-Earth orbit (LEO). LEO spacecraft imaging in visible-band mainly rely on the sunlight reflex (scattered) from the target surface. It is difficult to observe the target during the earth shadow, or during the daytime because of the strong skylight background. Infrared imaging can meet demand with all-day detection of spacecraft, be able to provide temperature characteristics of spacecraft with density distribution, and provide support for spacecraft on-orbit operation and fault analysis. In the long-wavelength infrared band region affords the highest SNRs over the 200–350 K temperature range exhibited by most space targets.

Generally, the *F*-number of ground-based imaging telescope system should satisfy with the Nyquist sampling. For the infrared wavelength of 3 μm and detector pixel size of 15 μm, the airy disk radius should be:

$$1.22 \times \lambda \times F \geqslant 30\ \mu\text{m} \tag{1}$$

where λ is the imaging wavelength, F is the *F*-number of the optics.

According to above mathematical relationship, we can come to a conclusion that the *F*-number of MWIR imaging is about 8. It is generally considered that the SNR of large *F*-number MWIR imaging for space targets is low, relevant studies have not been yet reported.

* Corresponding author.
E-mail address: a1032510210@126.com (Y. Liu).

http://dx.doi.org/10.1016/j.infrared.2014.08.001
1350-4495/

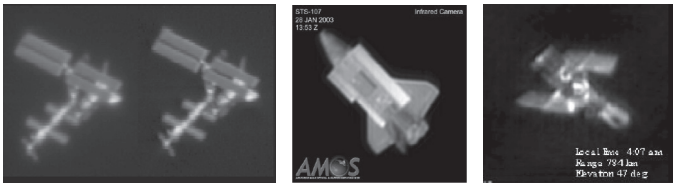

Fig. 1. Visible-band, long-wavelength thermal infrared and near-infrared images of LEO space target: (a) International Space Station; (b) STS-107 (Columbia); (c) Hubble Space Telescope.

Furthermore, cameras operating in the thermal infrared use a cold stop that is designed to match the exit pupil of the optics and thus avoid parasitic radiation. The detector array and cold stop are usually enclosed together in a small dewar assembly. So the cold stop of infrared camera is fixed, and the *F*-number of commercial off-the-shelf units is 2 or 4 with internal cold stop [4]. The orbit altitude of LEO spacecraft is about hundreds of kilometers above the ground, which imagery only accounts for a small proportion of detector pixels. Shown in Fig. 2 are relatively blurred MWIR images acquired with *F*/2 optics of meter-class telescope system. Recently, superresolution imaging with limited capacity is used to enhance the blurred images induced by undersampling [5,6].

To achieve large *F*-number infrared imaging, the approaches are:

(1) Cold stop matched

The height of micro infrared Dewar is increased, or the diameter of cold stop is reduced, the infrared camera with large *F*-number stop can be achieved. Alternatively, the cold stop is obviously set far away from the detector array, optical components and the cold stop are integrated in a larger infrared Dewar with cooling [7].

(2) Warm stop matched

The stop which temperature be the same as ambient air is set outside of the infrared camera, the distance between the stop and the detector array is increased, so the infrared camera with large *F*-number stop can also be nominal achieved. To minimize thermal radiation of the warm stop, the low emissivity material and curved shape are applied on it [8].

The former approach is comparatively costly, but the imaging effect can be better.

The spacecraft itself has potentially a very complex signal, due to its geometry for both reflected and emitted light [9]. We simplify this for our model and consider the case of a spherical spacecraft with diffuse reflectance. The solar radiation reflected by the spacecraft is:

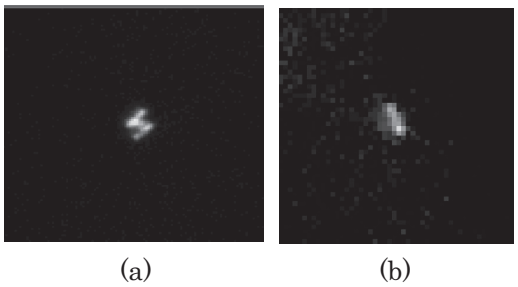

Fig. 2. The MWIR images of International Space Station (a) and Tian-gong (b) acquired during the nighttime with *F*/2 optics.

Table 1
Nominal Telescope system parameters used in simulation.

Parameter	MWIR channel
Location	CHANG CHUN
Latitude/longitude	43.85 N 125.40 E
Altitude	200 m
Time	Day and night
Spacecraft model	70 m^2, 1200 km
Phase angle	0°, 30°, 60°, 90°, 120°
Equivalent temperature	200–350 K
Telescope diameter	1.2 m
Obscuration diameter	0.3 m
Model atmosphere	Midlatitude summer
F-number	8 (internal cold stop *F*/4 & *F*/8)
Bandpass	3.7–4.8 μm
Optics transmission	0.8
IFOV	1.56 μrad
Pixel size	15 μm
Quantum efficiency	0.5
FPA readout noise	400 e-rms
Dark current	6.4e4 e-/pix/s
Integration time	15 ms

$$L_0 = \rho E_0/\pi \cdot p(\phi) \tag{2}$$

where ρ is target reflectivity, E_0 is solar irradiance at the edge of Earth's atmosphere, ϕ is phase angle, $p(\phi)$ is phase angle correction factor, specifically expressed as:

$$p(\phi) = \frac{2}{3\pi} \cdot [\sin\phi + (\pi - \phi)\cos\phi] \tag{3}$$

If we consider a telescope, the power incident on one pixel of the focal plane from the object during the exposure time is expressed in electron count as:

$$S_M = \frac{\eta t_{int}\lambda}{hc} \frac{\pi A_d L_M \tau_a \tau_o K(1-\varepsilon^2)}{4F^2} \tag{4}$$

where η is the quantum efficiency, t_{int} is the integration time, h is the Plank constant, c is the speed of light, A_d is the area of the detector pixel, L_M is the radiance from the object, including the target itself radiance and reflected solar radiance, τ_a is the atmospheric transmission, τ_o is the transmission of the optics, K is the imaging diffusion coefficient, ε is the obscuration ratio of the telescope primary mirror.

Similarly, the mean number of photo-electrons generated by the background in this pixel during the exposure time is equal to:

$$S_B = \frac{\eta t_{int}\lambda}{hc} \frac{\pi A_d L_B \tau_a \tau_0 (1-\varepsilon^2)}{4F^2} \tag{5}$$

where L_B is the radiance from the background, including sky background radiance and near-field radiance of the optics.

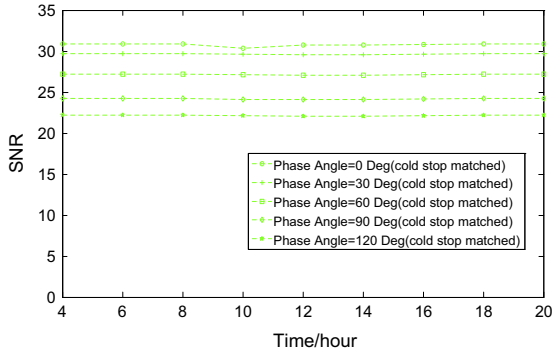

Fig. 3. The SNR vs. look time for MWIR imaging.

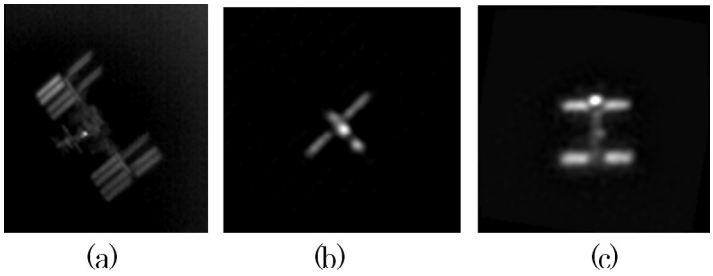

Fig. 5. The MWIR images acquired with large *F*-number optics: (a) International Space Station during near terminator; (b) Tian-gong during the night; (c) Tian-gong combination with Shen-shi during the daytime.

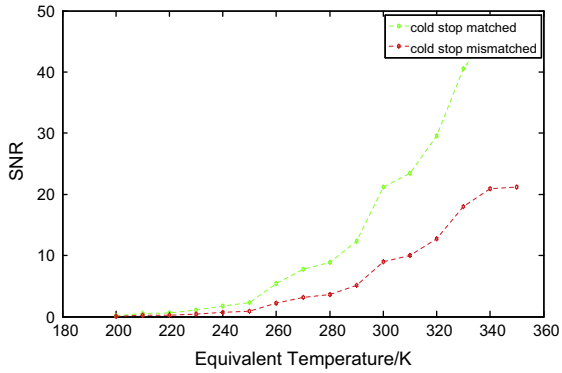

Fig. 4. The SNR vs. target equivalent temperature for MWIR imaging.

Infrared detector noises include photon noise, readout noise, dark current noise and non-uniform noise [10]. Non-uniform noise for each pixel of the focal plane is expressed in electron count as:

$$\overline{n_{FPN}} = U \cdot (S_M + S_B) \tag{6}$$

In the integration time, the SNR can be expressed as:

$$\mathrm{SNR} = \frac{S_M}{\sqrt{S_M + S_B + (\overline{n_{FPN}})^2 + \sigma_R^2 + t_{int} D_e}} \tag{7}$$

where σ_R is the RMS number of read noise electrons per pixel per readout in the detector, D_e is the dark current in electrons per pixel per second.

We first conduct a simulation analysis to assess the feasibility of using one meter-class telescope for spacecraft imaging in the MWIR band. The experiment telescope is located in Changchun Institute of Optics, Fine Mechanics and Physics, Chinese Academy of Sciences, a detailed listing of the parameters used in the simulation is in Table 1.

A plot of the dependence of the SNR on look time and target temperature is shown in Figs. 3 and 4.

In fact, the SNR of MWIR imaging is higher than the simulation results during the daytime, firstly the skylight background does not almost change over time in the MWIR band, secondly the temperature of space targets in the sunshine ozone is higher, leading to strong thermal radiation relatively, finally the space targets also reflect a portion of sunlight in the MWIR band. MWIR imaging sensor for some low temperature space targets that are in the shadow of the earth, will not be an effective detection means.

On this basis, we have developed a infrared camera with large *F*-number stop (*F*-number 8, format 640 × 512, pixel size 15 μm), which has been successfully applied on a 1.23 m telescope. The images of International Space Station and other extended targets are successfully acquired by the 1.23 m telescope during typical time, Fig. 5 shows the experimental results.

In conclusion, MWIR imaging sensor with large *F*-number stop is an important part of ground-based OE telescope for spacecraft detection. The simulation and experimental results show that MWIR imaging with large *F*-number optics for LEO spacecraft during the daytime and terminator is feasible, and imaging results are satisfactory beyond imagination. Application of cold stop matched approach, cold optics technology, adaptive optics with near-infrared wavefront sensor when the effects of atmospheric conditions are severe, and the original images undergone post-processing enhancement are strongly recommended.

The authors would like to thank Electro-Optical Detection Department, Changchun Institute of Optics, Fine Mechanics and Physics, Chinese Academy of Sciences, for providing 1.23 m experiment telescope. The work was supported by the National "863" Program of China.

Conflict of interest

The authors have declared that no conflict of interest exists.

References

[1] Mark Bolden, Air force Maui optical & supercomputing site tutorial, in: Proceedings of the Advanced Maui Optical and Space Surveillance Technologies Conference, Wailea, Maui, Hawaii, September 14–17, 2007.
[2] Michael L. Vigil, David J. Witte, Paul D. LeVan, Patricia J. Wallentine, David E. Briscoe, Danny L. Anderson, Sensor suite for the advanced electro-optical system (AEOS) 3.6-m telescope, Proc. SPIE 2819 (1996) 151–169.
[3] David C. Dayton, Mary Jo Duncan, John D. Gonglewski, Performance simulations of a daylight low-order adaptive optics system with speckle postprocessing for observation of low-earth orbit satellites, Opt. Eng. 36 (1997) 1910–1917.
[4] Nahum Gat, Jingyi Zhang, Ming De Li, Liang Chen, Hector Gurrola, Variable cold stop for matching IR cameras to multiple f-number optics, Proc. SPIE 6542 (2007) 65420Y.
[5] Keith Krapels, Ronald G. Driggers, Eddie Jacobs, Stephen Burks, Susan Young, Characteristics of infrared imaging systems that benefit from super resolution reconstruction, Appl. Opt. 46 (2007) 4594–4603.
[6] R. David Gerwe, David J. Lee, Jeffrey D. Barchers, Supersampling multiframe blind deconvolution resolution enhancement of adaptive optics compensated imagery of low earth orbit satellites, Opt. Eng. 41 (2002) 2238–2251.
[7] M. Dolci, A. Valentini, M. Ragni, A. Di Cianno, G. Di Rico, O. Straniero, D. Romano, J.-M. Christille, A. Piluso, AMICA at Dome C: results from the first year of automatic operation tests in Antarctica, Proc. SPIE 8446 (2012) 844645.
[8] Apostolos Deslis, Optical design of a warm shield for the 8–12 micron wavelength region, Proc. SPIE 6288 (2006) 628803.
[9] Hongyuan Wang, Wei Zhang, Fugang Wang, Infrared imaging characteristics of space-based targets based on bidirectional reflection distribution function, Infrared Phys. Technol. 55 (2012) 368–375.
[10] R. Hardie, F. Baxley, B. Brys, P. Hytla, Scene-based nonuniformity correction with reduced ghosting using agated LMS algorithm, Opt. Exp. 17 (2009) 14918–14933.